Chemical Engineering Journal 162 (2010) 565–572

Contents lists available at ScienceDirect

Chemical Engineering Journal

journal homepage: www.elsevier.com/locate/cej

Biosorption of manganese onto chitin and associated proteins during the treatment of mine impacted water

Mary Ann Robinson-Lora, Rachel A. Brennan*

Department of Civil and Environmental Engineering, The Pennsylvania State University, 212 Sackett Building, University Park, PA 16802, USA

ARTICLE INFO

Article history:
Received 6 December 2009
Received in revised form 28 May 2010
Accepted 31 May 2010

Keywords:
Acid mine drainage
Passive treatment
Remediation
Adsorption
Manganese
Crab-shell
Chitin

ABSTRACT

The manganese removal capacity of two purities of crab-shell chitin was evaluated under different pH conditions by means of kinetic tests and sorption isotherms. Demineralized (DM-SC20) and demineralized/deproteinized (DMP-SC20) crab-shell chitin were tested and compared to evaluate the contribution of chitin and its associated proteins to biosorption. The kinetics of manganese adsorption onto both types of solids was well described by the pseudo-second order model. The adsorption rates depended on the pH of system and the type of solid, with faster changes occurring under alkaline conditions and with DMP-SC20 (k_2 = 0.411–0.535 g/mg min) than with DM-SC20 (k_2 = 0.125–0.197 g/mg min). The adsorption equilibrium isotherms were best fit by the Langmuir, rather than Freundlich, model. The maximum sorption capacity (q_m, mg/g) was found to depend greatly on the pH of the solution, with minimal or no sorption observed at pH <5. At higher pH regimes, q_m values ranged from 0.165 (at pH 5.4) to 0.981 (at pH 8.7) for "pure" chitin (DMP-SC20) and increased from 0.878 (at pH 5.2) to 5.437 (at pH 8.6) when both chitin and protein were present (DM-SC20). Results clearly suggest that the chitin-associated proteins offer additional sorption sites for manganese.

1. Introduction

Manganese is a common contaminant found in mine impacted waters (MIW) derived from coal and metal mining [1]. In untreated MIW, manganese concentrations can vary considerably, from <1 mg/L to hundreds of mg/L, with an average of 10–25 mg/L [2]. When ingested or inhaled at high concentrations (>10 mg/day), this metal has been observed to cause neurological disorders in humans [3]. Although it is typically found at lower concentrations in MIW and has a lower toxicity than most of its other metal co-contaminants, Mn still affects the appearance, taste, and odor of water [4]. For these reasons, discharges from mining activities to surface water in the USA must comply with National Pollution Discharge Elimination System (NPDES) of the Clean Water Act, which limits the monthly average dissolved Mn concentration in the effluent to 2 mg/L. Even more stringent limits exist in the UK, with an Environmental Quality Standard set at 0.03 mg/L (annual average).

Over the last three decades many treatment technologies have been developed to address and correct the deleterious effects of mining on the quality of natural streams. However, among the possible contaminants found in MIW, Mn has been found notoriously difficult to remove [4,5]. The most common approach for the removal of Mn is its oxidation followed by its precipitation as manganese oxide (MnO_2). However, this requires high pH since abiotic and biological oxidation rates are slow for pH < 8.0, and can also be inhibited by the presence of Fe [4], the most prevalent metal contaminant in coal mining discharges. In addition, under reducing conditions, partial manganese removal has been reported and attributed to its precipitation as rhodochrosite ($MnCO_3$) [6].

In recent studies, crab-shell chitin has shown relatively high efficiency to remove Mn under reducing conditions from MIW in both laboratory and field studies [7–10]. This efficient acidity and metal removal may be attributed to the dissolution of chitin-associated carbonates, which are naturally present in the shells of crabs and other crustaceans to provide structural strength [11]. The role of chitin-associated minerals was previously evaluated, and results point to an enhanced dissolution of calcite, followed by a fast precipitation of manganese carbonates and/or phosphates (i.e.: $MnCO_3$ and $MnHPO_4$) [12]. In other treatment systems, adsorption has been identified as an important method of metal sequestration, especially under moderately acidic conditions. At initial stages, sorption onto the organic substrate or onto Al-Fe-(oxy)hydroxides has been observed [13–16]. Although most authors agree on the fact that this biosorption could be a transient phenomenon, results show a great sorption capacity for a variety of substrates, and some authors have recently suggested that it be used as the sole mechanism for remediation of MIW. Inexpensive sorbents like fly ash, red mud, pine bark, bentonite, zeolites [17], palm fruit bunch, maize cob [18], vegetable compost [13], lignite [19], and rice husk [20] have been tested

* Corresponding author. Tel.: +1 814 865 9428; fax: +1 814 863 7304.
E-mail address: rbrennan@engr.psu.edu (R.A. Brennan).

1385-8947/$ – see front matter © 2010 Elsevier B.V. All rights reserved.
doi:10.1016/j.cej.2010.05.063

with promising results. Utgikar et al. [21] also suggested applying metal adsorption as a preliminary step to decrease metal concentrations prior to biological sulfate reduction to prevent microbial inhibition due to metal toxicity.

The aim of this study was to evaluate the role of chitin and its associated proteins in the removal of manganese from MIW, due to sorption processes, under abiotic and anoxic conditions. The performance of two different purities of crab-shell chitin (demineralized, DM-SC20, and demineralized/deproteinized, DMP-SC20) was assessed and compared under different pH regimes. This study was conducted in an effort to develop a better understanding of the mechanisms that drive the observed changes in systems treated with a complex material, such as crab-shell chitin, where oxidation of this metal is limited.

2. Materials and methods

2.1. Chemicals

All chemicals used in this study were of reagent grade or higher quality. Ultra High Purity argon gas (UHPAG) was purchased from MG Industries (Malvern, PA). ChitoRem® SC-20 (minimally processed crab shell), derived from Dungeness crab (JRW Bioremediation, LLC, Lenexa, KS), was used as an example of chitinous material, and was purified further as follows. ChitoRem® SC-20 from the manufacturer was rinsed with deionized water to remove readily soluble salts and then demineralized using 1N HCl, according to protocols described in previous studies [11]. The completion of the reaction was followed by measuring the pH of the supernatant until the pH remained acidic and stable after a new addition of the hydrochloric acid solution. Particles were then washed with deionized water until neutrality of the rinsate (monitored by pH measurement), and dried overnight at 50 °C. The obtained demineralized material (DM-SC20) was sieved using sieves no. 7 and 140 to remove big particles (>2.80 mm) and fines (<0.106 mm), resulting in a particle distribution representative of ~82% of the original SC-20 material [22]. A fraction of the obtained DM-SC20 was deproteinized using 1N NaOH [11] while measuring the absorbance of the supernatant at 280 nm until it reached a maximum plateau, indicating the completion of the reaction. Particles were then washed with deionized water until neutrality of the rinsate, and dried and sieved as above to produce the demineralized and deproteinized product, DMP-SC20.

2.2. Characterization of particles

The chemical composition of all solids was determined by lithium metaborate fusion followed by ICP-AES analyses (Perkin-Elmer Optima 5300) at the Materials Characterization Laboratory at The Pennsylvania State University. Rock standards were used to calibrate the results. The total carbon and nitrogen of the obtained solids were analyzed in duplicate by combustion, using a Fisons NA 1500 Elemental Analyzer, at the Agricultural Analytical Services Laboratory at the Pennsylvania State University. The surface area of the solids was measured in duplicate by physical adsorption of N_2 and calculated using the BET (Brunauer, Emmett and Teller) method with a Micrometrics Instrument Corporation ASAP 2020. Sample morphology was observed using a FEI Quanta 200 environmental scanning electron microscope (ESEM).

Acid–base discontinuous titrations were performed in singlet at a constant ionic strength (0.1 M $NaNO_3$), using a separate portion of the solids (2 g/L DM- or DMP-SC20) for each point of the curve. A known amount of HCl was added to set the initial pH < 3 and then a standardized NaOH solution was used as titrant. The final pH was measured after a contact time of 3 h. This rather long contact time was found to be necessary to obtain a stable pH reading. The choice for the down-up titration and the use of one sample per point was based on results from preliminary attempts to characterize these solids in our laboratory that suggested their instability at pH >10. Indeed, deproteination can occur with alkali treatment [11]. Therefore, this experimental setup was found to be adequate to minimize changes in the solids during the characterization.

2.3. Synthetic MIW (SMIW) solutions

Manganese removal tests were conducted using synthetic MIW (SMIW) to limit the affect of other metals (likely present in natural MIW) on the results. To better imitate the conditions found in MIW, solutions were prepared using Na_2SO_4 (1.4 g/L or 10 mM) as the background salt. The initial pH was adjusted to the desired value by adding appropriate amounts of 1N H_2SO_4 or 1N NaOH. Solutions were deaerated with UHPAG for 2–3 h, and then appropriate amounts of $Mn(NO_3)_2$ were added to adjust the initial Mn concentration to the desired value. Prior to use, solutions were equilibrated in an anaerobic chamber (Coy Laboratory Products, Inc., Grass lakes, MI) for at least 24 h.

2.4. Kinetic tests

Kinetic tests were conducted to evaluate manganese removal rates under different pH regimes (low, pH ~ 5, and high, pH ~ 9), with an initial Mn concentration of 10 mg/L. Reactors (400 mL) were operated inside an anaerobic chamber with continuous stirring at 500 rpm to ensure complete suspension of the solids. A fixed solid load of 5 g/L (DM- or DMP-SC20) was used, which was added at $t = 0$. The pH was continuously monitored and duplicate samples (10 mL) were taken at predetermined time intervals of $t = 0$, 10, 20, and 30 min, and at 1, 2, 6, 12, 24, 48, and 72 h. Samples were filtered (0.2 μm), diluted (1:10), and preserved in acidified-anoxic deionized water (2 mL/L conc. HNO_3) for Mn analyses.

2.5. Batch sorption tests

Manganese sorption onto DM- and DMP-SC20 was evaluated in closed systems, as a function of equilibrium pH (pH 5 to pH 9) and Mn concentration (0.5–250 mg/L). Systems were prepared in duplicate inside an anaerobic chamber, by mixing 20 mL of sterile (filtered, 0.2 μm), anoxic SMIW with 0.1 g of DM- or DMP-SC20 in acid-washed glass vials. Blank systems (without the addition of solids) were prepared in singlet. Vials were sealed and continuously stirred on an orbital shaker for 72 h. The 72-h contact time was chosen based on preliminary tests conducted in our laboratory to ensure that all chemical transformations in the systems were completed. After the contact time was elapsed, the vials were opened and the pH of the solution immediately measured inside the anaerobic chamber. Samples were filtered (0.2 μm), diluted (1:10), and preserved in acidified-anoxic deionized water (2 mL/L conc. HNO_3) for Mn analyses. The concentration of manganese sorbed onto the solid (q_e, mg/g) was calculated using Eq. (1):

$$q_e = \frac{C_0 - C_f}{a} \quad (1)$$

where C_0 and C_f are the initial and final concentration of manganese in solution (mg/L), respectively, and a is solid load used (g/L).

Attenuated Total Reflectance Fourier Transform Infrared (ATR-FTIR) spectrometry (Bruker Optics IFS 66/S, Germany) was used to identify the functional groups involved in the Mn adsorption. For each type of solid, three conditions were selected for analysis: (1) equilibrated at pH 5, (2) equilibrated at pH 9, and (3) after Mn adsorption at pH 9. The selected solid samples were pressed into a self-supporting disk using a 7 mm stainless steel dye and hand

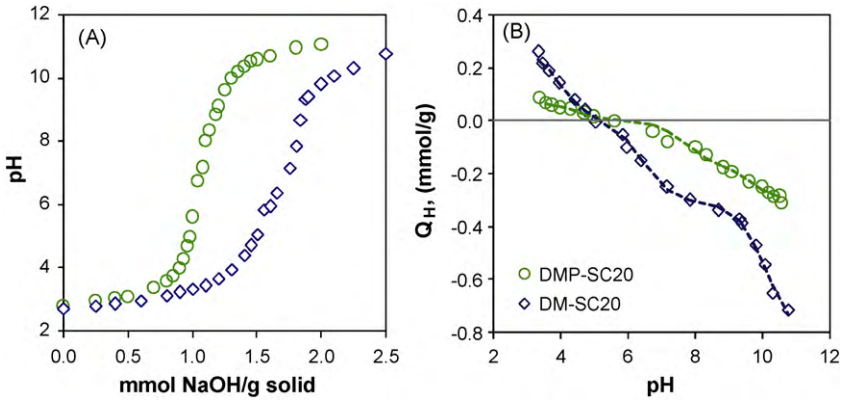

Fig. 1. Potentiometric characterization of DMP- and DM-SC20: (A) Alkalimetric titration of solids and (B) net-negative surface charges calculated from titration curves. Dotted lines correspond to three-site model prediction.

press. These disks were then pressed onto a ZnSe ATR crystal for analysis at an angle of incidence of 45° degrees. The spectra were obtained from 800 to 4000 cm^{-1} at a resolution of 6 cm^{-1} with an accumulation of 400 scans.

2.6. Analytical methods

The pH was measured using a hand-held VWR® sympHony® pH meter provided with a Gel 3-in-1 electrode. Daily calibrations were carried out using buffers of pH 4, 7, and 10 and slopes were consistently greater or equal to 98.5% of the Nernst value. Dissolved metal concentrations were measured by inductively coupled plasma emission spectrometry (ICP, Leeman Labs PS3000UV) at the Materials Characterization Laboratory at The Pennsylvania State University.

Statistical analyses of the collected data were performed using MINITAB® statistical software (Minitab Inc., State College, PA). The geochemical computer program PHREEQC [23] was used to estimate the speciation of manganese in solution. The concentrations of nitrate released from the added metal salts were estimated based on the initial, measured concentration of their associated metals.

3. Results

3.1. Characterization of solids

Results from the chemical analyses indicate that both solids are mainly composed of carbon and nitrogen, with almost negligible (< 0.4%) residues of chitin-associated minerals (Supplemental Table 1). The measured carbon (44.3 ± 1.5%) and nitrogen (6.9 ± 0.1%) contents in DMP-SC20 are very close to the theoretical values for pure chitin ($C_8H_{15}O_5N$, 46.8% C and 6.9% N). Higher C and N contents were found in DM-SC20 (46.2 ± 0.8 and 10.5 ± 0.1%, respectively). The percentage of protein in DM-SC20 can be estimated based on its nitrogen content using Eq. (2) [11]:

$$\%\,\mathrm{Prot} = 6.25(\%N - 6.9) \tag{2}$$

where %Prot is the percentage of proteins, %N is the percentage of nitrogen, and 6.25 and 6.9 correspond to the theoretical percentage of nitrogen in protein and chitin, respectively. Therefore, the percentage of proteins in DM-SC20 corresponds to ~23%. SEM micrographs (Supplemental Fig. 1) reveal a somewhat similar structure of both materials, consisting of a series of stacked layers with limited visible porosity. Low porosity was further indicated by the low surface area measurements obtained by BET analysis (2–3 m^2/g), with no significant difference between the two solids (Supplemental Table 1).

Titration results for both DMP- and DM-SC20 indicate the presence of at least two inflection points (Fig. 1A). The end points of the titrations were estimated based on the graphic method proposed by Gran referenced in [24], and the total active sites corresponded to 0.3 and 0.8 mmol/g for DMP- and DM-SC20, respectively. The net surface charge (Q_H, mmol/g) as a function of the pH of the suspension was calculated using Eq. (3) [24]:

$$Q_H = \frac{C_A - C_B + [\mathrm{OH}]^- - [\mathrm{H}^+]}{a} \tag{3}$$

where C_A and C_B are the molar concentrations of the acid and the base, respectively, in the suspension after each titrant addition, and a is solid load used (g/L). Net-negative charges were observed on the solids when pH > 5.6 for DMP-SC20 and pH > 5.1 for DM-SC20 (Fig. 1B). For a given pH value, surface charges were higher on DM-SC20.

Experimental data can be described assuming the solid surface consists of a discrete number of weakly monoprotic acidic sites ($\equiv S_i$) that dissociate according to Eqs. (4) and (5):

$$\equiv S_iH \Leftrightarrow \equiv S_i^- + H^+ \tag{4}$$

$$K_{app,i} = \frac{[\equiv S_i^-][H^+]}{[\equiv S_iH]} \tag{5}$$

where $\equiv S_iH$ and $\equiv S_i^-$ are protonated and deprotonated species of the ith type of acidic site, and $K_{app,i}$ is the apparent deprotonation constant [25,26]. Combining the mass balance for the ith acidic site with Eq. 5 it is possible to relate $[\equiv S_i^-]$ to the pH of the system and the constant parameters $K_{app,i}$ and $[\equiv S_i]_T$:

$$[\equiv S_i]_T = [\equiv S_i^-]\left(\frac{1 + [H^+]}{K_{app,i}}\right) \tag{6}$$

Therefore, the net-negative charge concentration on the solid can be expressed as:

$$Q_H = \sum_i [\equiv S_i^-] = \sum_i \frac{[\equiv S_i]_T}{1 + [H^+]/K_{app,i}} \tag{7}$$

For the present study, three different acidic sites were assumed to be present on the evaluated solid. A non-linear regression method was performed to fit the data obtained from the alkalimetric titrations and estimate the six adjustable parameters ($[\equiv S_1]_T$, $[\equiv S_2]_T$, $[\equiv S_3]_T$, $K_{app,1}$, $K_{app,2}$, $K_{app,3}$, Table 1). High correlation coefficients and low standard errors were obtained for both types of solids, indicating that the three-site model (represented by the dotted lines in Fig. 1B) describes the experimental data well. The estimated concentration of the acidic sites is always higher for DM- than for DMP-SC20.

Table 1
Adjustable parameters for three-site model from non-linear regression of titration data.

Solid	$[\equiv S_1]_T$ (mmol/g)	$[\equiv S_2]_T$ (mmol/g)	$[\equiv S_3]_T$ (mmol/g)	$pK_{app,1}$	$pK_{app,2}$	$pK_{app,3}$	r^2	s_e
DMP-SC20	0.07	0.17	0.14	4.46	7.71	9.68	0.999	0.015
DM-SC20	0.28	0.31	0.51	3.96	6.45	10.11	0.998	0.015

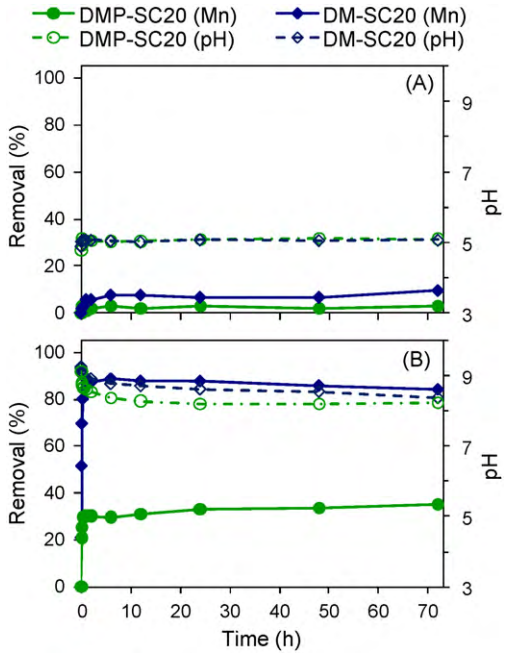

Fig. 2. Manganese uptake onto DMP- and DM-SC20 under (A) acidic and (B) alkaline conditions. Data points represent averages of duplicate samples; error bars are smaller than the symbol size.

3.2. Kinetic tests

Kinetic tests were conducted to evaluate the metal removal rates by the solids under both low and high-pH regimes, with an initial manganese concentration of 10 mg/L. Qualitatively, a similar behavior was observed in all the evaluated systems. The majority of the Mn removal occurred during the first 6 h (Fig. 2). However, slight changes (increased and decreased removal) were observed to occur throughout the duration of the tests, especially in those systems treated with DM-SC20. Nevertheless, those changes did not lead to significantly different removals (p-value = 0.4) than the calculated average for $t \geq 6$ h. Under low-pH conditions (pH ~ 5), Mn uptake by both types of solids was observed to be very low (Fig. 2A), as expected due to the limited amount of negative sites at low pH. After a contact time of 72 h, only 3 and 10% of the initial manganese in solution (Mn_o = 10 mg/L) was removed by DMP- and DM-SC20, respectively. In contrast, higher amounts of manganese were removed by both types of solids under high-pH conditions (pH ~ 9, Fig. 2B). After 72 h, 35 and 83% Mn was removed by DMP- and DM-SC20, respectively.

Along with manganese removal, the addition of the evaluated solids also caused changes in the pH of the solution. These changes were faster, yet smaller, under low-pH conditions (from pH 4.8 to pH 5.1 in less than 30 min), than under high-pH conditions (from pH 9.2 to pH 8.2 by the end of the tests).

3.3. Manganese adsorption isotherms

Sorption data were interpreted in terms of the Langmuir (Eq. (8)) and the Freundlich (Eq. (9)) sorption models:

$$q_e = q_m \frac{K_L C_e}{1 + K_L C_e}. \quad (8)$$

$$q_e = K_F C_e^{1/n} \quad (9)$$

where q_e and C_e are the equilibrium concentration of the adsorbate on the solid (mg/g) and in the liquid phases (mg/L), respectively; q_m is the maximum adsorption capacity (mg/g) according to the Langmuir model; K_L, K_F, and n are constants. Based on the correlation coefficients (Table 2), the data show a good agreement with the two models. However, the obtained fitted curves for the Freundlich model have higher standard errors (s_ε) and over-predict the sorption capacity of the solids at high metal concentrations. For this reason, the Langmuir model (represented by solid lines in Fig. 3) was chosen as the best fit to describe the data.

For both types of solids, the extent of manganese removal strongly depended on the pH of the system (Fig. 3). However, as the pH of the solutions increased, this pH-dependency decreased. At low-pH regimes, a 30-fold decrease in the hydronium ion concentration (i.e. from pH 5.2 to pH 6.7) resulted in a 3-fold increase of the maximum adsorption capacity (q_m). At high-pH regimes, a 10-fold decrease in the hydronium ion concentration (i.e. from pH 7.6 to pH 8.6) resulted in only a 10% increase of q_m. In addition, for the same pH regime, the adsorption capacities of DM-SC20 were 5.3–7.3 times higher than those calculated for DMP-SC20.

Similar ATR-FTIR spectra were obtained from both solids at all the evaluated conditions (Fig. 4). Bands in all spectra are in close agreement to those previously reported for α-chitin extracted from crustacean shells [27,28]. This is especially true for DMP-SC20 samples. However, certain differences were found in DM-SC20 with respect to the pure material (compare Fig. 4A–C to Fig. 4D–F). Although relatively minor, spectra from samples of the same type of solid also exhibited some differences between each other as a result of the different treatment conditions.

Table 2
Results obtained from the fitting of the isotherms to Langmuir and Freundlich adsorption models.

Solid	pH	Langmuir model				Freundlich model			
		q_m	K_L	r^2	s_e	K_F	n	r^2	s_e
DMP-SC20	5.4	0.165	0.085	0.995	0.011	0.008	1.268	0.849	0.036
	6.9	0.446	0.120	0.998	0.023	0.058	2.133	0.891	0.080
	7.9	0.900	0.307	0.857	0.054	0.198	2.631	0.871	0.201
	8.7	0.981	0.440	0.876	0.058	0.252	2.877	0.873	0.279
DM-SC20	5.2	0.878	0.016	0.946	0.151	0.022	1.370	0.950	0.340
	6.7	3.271	0.133	0.980	0.395	0.353	1.920	0.913	1.046
	7.6	4.972	0.340	0.970	0.333	0.863	2.282	0.942	1.719
	8.6	5.437	0.439	0.963	0.298	1.279	2.697	0.908	1.473

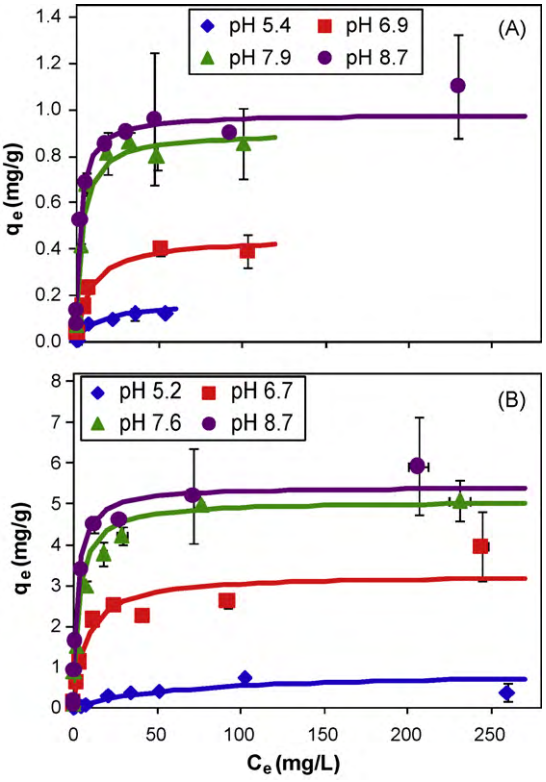

Fig. 3. Manganese adsorption onto 5 g/L of (A) DMP-SC20 and (B) DM-SC20 at different pH values. Data points represent duplicate averages; error bars represent one standard deviation. Solid lines correspond to Langmuir fitting model.

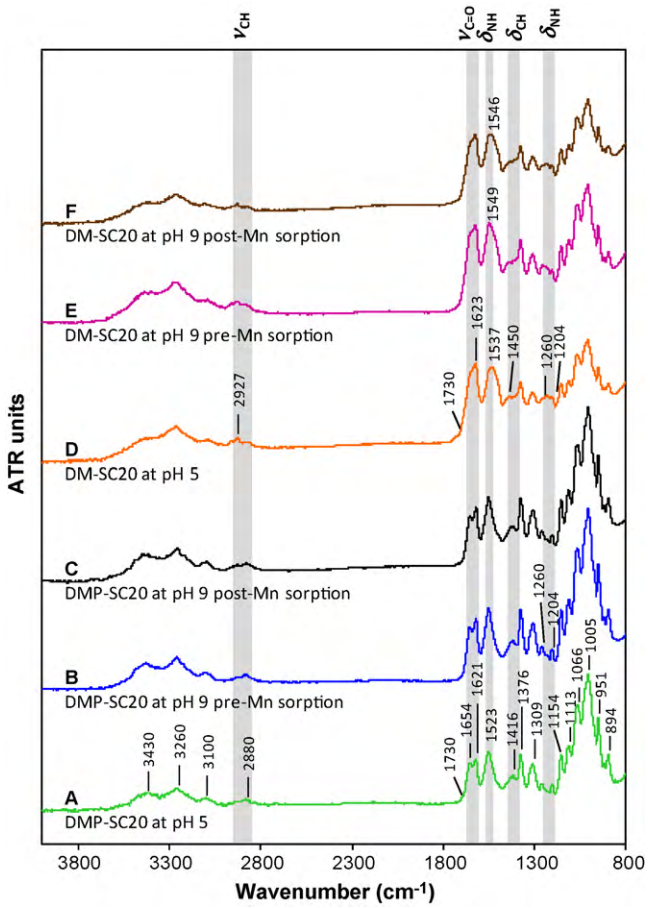

Fig. 4. ATR-FTIR spectra of DMP-SC20 equilibrated at pH 5 (A) and before (B) and after (C) Mn sorption at pH 9, and DM-SC20 equilibrated at pH 5 (D) and before (E) and after (F) Mn sorption at pH 9. Shaded areas correspond to wavenumber regions associated with stretching (ν) and bending (δ) vibrations of the indicated bonds.

4. Discussion

4.1. Potentiometric titration of solid

Recent studies have evaluated the potential of chitin and chitosan (its deacetylated derivative) as sorption agents. Chitin and chitosan have both been shown to be excellent metal ligands for heavy metal complexation [30–34,46,47]. However, biosorption is a complex process that has not been very well understood since it can involve several mechanisms such as complexation, chelation, ion exchange, and physical adsorption. It has been suggested that the metal forms a coordination complex with the nitrogen or oxygen in chitin [29]. Numerous studies have shown the ability of chitinous materials to remove both cationic and anionic contaminants including not only metals (e.g. Cu, Co, Pb, Cd, Fe, Au, Se, Cr) but also sulfate [30–34]. Such studies are usually conducted with relatively pure chitin polymers, extracted from fungi or crustaceans. However, a few groups have recently evaluated the use of raw chitinous materials for the removal of metals [47,49,50].

In the present study, the sorption capacity of a rather complex material was studied. Crab shells are composed by chitin fibrils, arranged with a variety of proteins and clusters of minerals [35]. Several studies have reported the composition of chitin-associated proteins in crustaceans, by means of their amino acid residues [11,36,37]. With differences in their concentrations, aspartatic (pK 2.09, 3.86, and 9.82) and glutamatic acids (pK 2.19, 4.25, and 9.67), histidine (pK 1.82, 6.04, and 9.17), alanine (pK 2.35 and 9.69), lysine (pK 2.18, 8.95, and 10.53), tyrosine (pK 2.20, 9.11, and 10.07), and arginine (pK 2.17, 9.04, and 12.48) are commonly found in the evaluated organisms. However, the exact structure of chitin-associated proteins remains somewhat unknown. After demineralization, the obtained DM-SC20 particles consist of a mixture of chitin and its associated proteins. After the deproteinization process, it is believed that DMP-SC20 consists mainly of chitin: Percot et al. [11] reported protein residues < 0.6%. However, due to the intricate relationship between this biopolymer and the proteins, it is likely that some minor protein residues were still present in DMP-SC20. In addition, crustacean shells also contain small amounts of lipids and carotenoids, which were not removed during demineralization or deproteinization. Nevertheless, results from carbon and nitrogen analyses reveal that almost pure chitin was indeed obtained (Section 3.1).

The acid–base characteristics of sorption sites are important when determining the potential performance of a sorbent. Solid surface charge changes as a function of pH indicate the likelihood of cation adsorption. In the present study, the net-negative charges that were observed only for pH > 5.1 or 5.6 indicate that cation adsorption will be electrostatically inhibited under the typically low pH of MIW. On the other hand, the estimation of the pK_{app} of the potential sorption sites gives an indication of the functionality of those sites. In the case of chitinous materials, two main functional groups are expected to be present and responsible for adsorption. Each chitin monomer (N-acetylglucosamine) contains one carbonyl and one amine group. These two functional groups are also present in the chitin-associated proteins. In general, pK_a values for carboxylic acids range between 2 and 6, while for amines values are usually >8 [24]. Therefore, for DMP-SC20, the first site detected ($\equiv S_1$) is attributed to carboxylic groups, while the second and third ($\equiv S_2$ and $\equiv S_3$) are attributed to amine groups. Similarly, for DM-SC20, $\equiv S_1$ and $\equiv S_3$ correspond to carbonyl and amine groups, respectively. Although somewhat higher than the typical

Table 3
Kinetic parameters for pseudo-second order adsorption model.

	DMP-SC20 (chitin)		DM-SC20 (chitin + proteins)	
	pH 5.04 ± 0.07	pH 8.62 ± 0.14	pH 5.05 ± 0.02	pH 9.01 ± 0.14
q_e (mg/g)	0.063	0.643	0.179	1.875
k_2 (g/mg min)	0.411	0.535	0.125	0.197
r^2	0.871	0.999	0.991	1.000

value, pK_{app2} for DM-SC20 likely corresponds to a carboxylic group. The estimated concentration of sorption sites, based on the regression calculations, in DMP-SC20 (0.37 mmol/g) is greatly exceeded by DM-SC20 (1.10 mmol/g). These values are somewhat higher than those estimated from the graphic method (0.8 and 0.3 mmol/g for DM- and DMP-SC20, respectively). Given that the surface areas of the solids were not significantly different, the difference in the concentration of sites between DMP- and DM-SC20 is an indication that the chitin-associated proteins remaining in DM-SC20 play an important role in its overall sorption capacity.

4.2. Kinetic tests

These tests were conducted with two main purposes: (1) to evaluate manganese uptake rates and (2) to define an appropriate contact time to ensure that equilibrium had been reached for adsorption isotherms.

Several models have been tested to describe the kinetics of metal adsorption onto chitinous materials [38,39]. Among these models, the pseudo-first order (Eq. (10)), pseudo-second order (Eq. (11)), and intraparticle diffusion (Eq. (12)) models were selected and tested with the results obtained in this study:

$$\log(q_e - q_t) = \log\ q_e - \frac{k_1}{2.303}t \tag{10}$$

$$\frac{dq}{dt} = k_2(q_e - q_t)^2 \tag{11}$$

$$q_t = k_i t^{0.5} \tag{12}$$

where q_e and q_t are the adsorbate concentration in the solid (mg/g) at equilibrium and at time t (min), respectively, and k_1 (min^{-1}), k_2 (g/mg min), and k_i (mg/g min$^{0.5}$) are rate constants. To facilitate the evaluation, Eq. (11) was integrated and transformed into a linear form (Eq. (13)):

$$\frac{t}{q_t} = \frac{1}{k_2 q_e^2} + \frac{t}{q_e} \tag{13}$$

To minimize errors due to the changes observed at later times in the tests, the kinetic models were evaluated over the range of $t \leq 6$ h. Results of the linearized forms of the three evaluated models clearly show that the pseudo-second order model (Eq. (11)) is the best at describing the observed Mn adsorption. While very poor or no correlation was found for the pseudo-first order and the intraparticle model, correlation coefficients for the pseudo-second order model were close to one at pH 9 (Table 3). However, the reduced sorption observed at pH ~ 5 for DMP-SC20 did not fit the expected behavior, decreasing the correlation (r^2 = 0.871). The higher values of the rate constant obtained for DMP-SC20 suggest that manganese uptake is faster onto chitin than onto the chitin-protein mixture (present in DM-SC20). However, the higher q_e values obtained with DM-SC20, corroborates the idea that the chitin-associated proteins offer additional sites for manganese adsorption.

The extended duration of the kinetic experiments (72 h) was selected based on preliminary tests in our laboratory using chitinous materials where minimal or no changes were observed after 24–48 h. Although some changes were observed at later times in the tests presented here, statistical analysis indicates that the values measured for $t \geq 24$ h are not significantly different from each other. Therefore, the 72-h contact time can be considered appropriate to ensure that equilibrium was reached during this laboratory test. In field applications however, it is likely that lower sorption rates would be observed as agitation and shear regimes will likely be lower.

4.3. Manganese adsorption isotherms

The process of manganese adsorption onto DMP- and DM-SC20 is well described by the Langmuir model. The essential characteristics of the Langmuir model can be expressed in terms of the separation factor, R_L, a dimensionless parameter defined by Eq. (14) [40]:

$$R_L = \frac{1}{1 + K_L C_0} \tag{14}$$

where K_L is the Langmuir model constant and C_0 is the initial concentration. R_L indicates the characteristics of the adsorption: unfavorable for $R_L > 1$, linear for $R_L = 1$, favorable for $0 < R_L < 1$, and irreversible for $R_L = 0$. For this study, R_L values calculated for initial Mn concentrations between 0.5 and 250 mg/L were all between 0.01 and 0.99. This indicates a favorable adsorption of manganese onto both types of solids.

On the other hand, the sorption capacity of DMP-SC20 is greatly exceeded by that calculated for DM-SC20. As was mentioned before, this is an indication that the chitin-associated proteins present in DM-SC20 are greatly responsible for the observed removal of manganese. In this case, a change from ~100% chitin (in DMP-SC20) to ~0.3:1 protein-to-chitin content in DM-SC20 leads to an increase of sorption capacity of 5.3–7.3 times. This additional sorption capacity related to the chitin-associated proteins is due to the functional groups present in their constituent amino acids. Among the five most common amino acids found in the crustacean shells, two are acidic in character (aspartic and glutamic acids), each providing an extra carboxylic group, while other three are basic (histidine, lysine, and arginine), each providing an extra amine group. Under the conditions at which the tests were conducted (pH 5–9), it is expected that the carboxylic groups were deprotonized, while the amine groups were positively charged. At slightly low-pH conditions, it is likely that the hydronium ions out-competed the manganese in solution, limiting its binding to the amine groups and leaving the carboxylic groups primarily responsible for the observed adsorption. As the activity of the hydronium ions decreased under high-pH conditions, manganese was able to be sorb onto the available amine groups.

The collected ATR-FTIR spectra (Fig. 4) provide insights into the functional groups that were present and active during Mn adsorption. The close agreement found between the FTIR spectra of DMP-SC20 samples and those reported in literature [27,28] corroborates once more the fact that this material was indeed pure chitin. Samples of the same material appeared not to be affected by the different treatment conditions. This is especially true for DMP-SC20. It is possible that the little Mn removal obtained with this solid make changes in FTIR hard to detect. The only noticeable difference between the spectra of DMP-SC20 samples is the occurrence of a shoulder at ~1730 cm^{-1} for the sample equilibrated at pH

5. This feature (also noticeable for the DM-SC20 at pH 5) could be associated with vibration of carbonyl groups [41] and might have been enhanced by the slightly low pH of the system. Two of the main differences between DMP- and DM-SC20 spectra are associated with the amide I (C=O stretching ($\nu_{C=O}$) at 1660–1620 cm^{-1}) and amide II (N–H bonding (δ_{NH}) at 1550–1520 cm^{-1}) vibrations [28,42]. Since the peptide bond in proteins is in essence an amide, it is not surprising to find additional vibration bands associated to the presence of proteins in DM-SC20. The position of protein–amide bands is affected by the secondary structure [43]. Therefore, the observed shifts and unresolved shape of these bands are likely due to conformational changes associated with changes of H-bonds as well as the effect on Mn bonding. This constitutes additional evidence for the role of proteins in the removal of Mn. An additional difference between DMP- and DM-SC20 is the changes in intensity ratio in the 2930–2880 cm^{-1} region, associated with CH, CH_2, and CH_3 stretching vibrations (ν_{CH}) [43]. Such variations are therefore likely due to the different alkane sidechains of the chitin-associated proteins. The remarkable similarities between all spectra within the signature or fingerprint region (wavenumber < 1500 cm^{-1}) indicate that the chitin structure is the main component responsible for the shape and location of the observed bands. It is possible that the relatively low content of each type of protein in DM-SC20 resulted is low signals, barely detected by the instrument and masked by the stronger signals of chitin structure. However, some variations were detected in the regions of 1450–1430 and 1260–1204 cm^{-1}. The first of these regions corresponds to bending vibrations of the C–H bonds (δ_{CH}), while the latter corresponds to N–H bonding [27]. These additional, unresolved bands observed in the DM-SC20 spectra are likely due to particular features of the chitin-associated proteins and their secondary structure. Furthermore, the changes in the intensity ratio of the N–H bonding bands may also indicate conformational changes due to the pH conditions and the sorption of Mn.

Previous studies have evaluated the manganese removal capacity of several natural and synthetic sorbents [18,44,45]. In general, reported maximum sorption capacities ranged between 2 and 30 mg/g [18,44,45], with exceptionally high values observed for pecan nutshell (98 mg/g) and *Arthrobacter* sp. biomass (406 mg/g) [44]. Since all tests were conducted under different conditions, a direct comparison with the results obtained in this study cannot be made. However, qualitatively speaking, the maximum Mn adsorption capacities of DMP- and DM-SC20 appear to be within the lower end of the reported range (0.64 and 1.88 mg/g, respectively, Table 3). The very high sorption values reported with pecan nutshell and *Arthrobacter* sp. biomass are likely due to the abundance of negatively charged functional groups such as carboxylic acids and phenol in comparison to those found in chitin and its associated proteins. The relatively poor Mn sorption observed with pure chitin in this study also contradicts previous studies where metals like zinc, copper, cadmium, and lead were efficiently removed with sorption capacities ranging from 15 to 323 mg/g [46,47]. According to the Irving–Williams order, the complex stability of Mn^{2+} ions is well below those of the formerly mentioned transition metals [24]. The stability of Mn could explain the relatively low sorption observed here. In fact, the same behavior was also noticed with *Arthrobacter* sp. biomass: Mn uptake was the lowest in comparison to Pb, Cu, and Zn [44]. Another factor that could have negatively influenced the Mn sorption onto the evaluated solids was the presence of sulfate in the evaluated systems. The addition of sulfate to the SMIW was intended to better imitate the typical conditions found in affected streams. However, high levels of sulfate can lead to the formation of sulfate–manganese complexes. Thermodynamic calculations indicate that with 1000 mg/L of sulfate in solution, manganese speciation consists of ~73% as $Mn^{2+}_{(aq)}$ and ~27% as $MnSO_{4(aq)}$. Therefore, the occurrence of manganese complexation could have partially inhibited its sorption onto the evaluated chitinous materials.

The main objective of the present study was to evaluate the individual contributions of chitin and its associated proteins to manganese removal when using a complex substrate such as crab-shell particles. The results indicate that both chitin and protein are able to partially adsorb manganese. However, the presence of proteins significantly increases the sorption capacity of the material. For field applications, untreated crab-shell particles are the most cost-effective alternative. In this raw material, the proportion of protein-to-chitin has been reported as high as 1.2:1 [48], which greatly exceeds the one reported here (~0.3:1). Consequently, higher manganese removal due to sorption onto the protein sorption sites could be expected. On the other hand, the low pH values commonly found in MIW might inhibit this sorption process. However, chitin-associated carbonates (also present in crab shells) have proven to be an excellent source of buffering capacity, rapidly increasing the solution pH. As a result, it can be expected that the chitin-associated proteins will contribute to the removal of manganese, once the pH of the solution is increased due to the dissolution of chitin-associated carbonates.

5. Conclusions

The findings presented here demonstrate an important advantage of chitinous materials for the anaerobic treatment of manganese-bearing MIW. In previous studies, manganese removal was shown to be poor under anaerobic conditions [6,51], and field applications had to rely on an additional aerobic/oxidative treatment step to achieve the desired removal of this metal [1,4,5,51]. Results from the present study demonstrate the role of chitin and chitin-associated proteins in the removal of manganese from MIW under abiotic and anaerobic conditions. Both types of biomolecules are capable of sorbing manganese; however, the removal capacity of the chitinous materials significantly increases when chitin-associated proteins are present. The available sorption sites are likely associated with both carboxylic and amine functional groups. The adsorption equilibrium isotherms, well described by the Langmuir model, indicate that the maximum sorption capacity greatly depends on the pH of the solution. While essentially no sorption was observed at pH < 5, a 6-fold increase in the sorption capacity of both types of materials was observed when the pH changed from low (pH 5) to high (pH 9). It is likely, therefore, that sorption contributes to manganese removal as the pH is increased due to the dissolution of chitin-associated carbonates when raw crab shell is used in the treatment of MIW. More research is needed to evaluate the persistence and reversibility of this mechanism under continuous abiotic conditions.

Acknowledgements

This material is based upon worked supported by the National Science Foundation, CAREER Award No. CBET-0644983. Any opinions, findings, and conclusions or recommendations expressed in this material are those of the authors and do not necessarily reflect the views of the National Science Foundation. Three anonymous reviewers are thanked for their helpful comments to improve the manuscript.

Appendix A. Supplementary data

Supplementary data associated with this article can be found, in the online version, at doi:10.1016/j.cej.2010.05.063.

References

[1] K.B. Hallberg, D.B. Johnson, Biological manganese removal from acid mine drainage in constructed wetlands and prototype bioreactors, Sci. Total Environ. 338 (2005) 115–124.

[2] USEPA, Final 2008 Effluent Guidelines Program Plan [Online], 2008. Available at http://www.epa.gov/guide/304m/2008.

[3] USEPA, Integrated Risk Information System (IRIS) on Manganese. National Center for Environmental Assessment, 1999. Available at http://www.epa.gov/iris/subst/0373.htm.

[4] K.L. Johnson, P.L. Younger, Rapid manganese removal from mine waters using an aerated packed-bed bioreactor, J. Environ. Qual. 34 (2005) 987–993.

[5] P.L. Sibrell, M.A. Chambers, A.L. Deaguero, T.R. Wildeman, D.J. Reisman, An innovative carbonate co-precipitation process for the removal of zinc and manganese from mining impacted waters, Environ. Eng. Sci. 24 (2007) 881–895.

[6] S.G. Benner, D.W. Blowes, W.D. Gould, R.B. Herbert Jr., C.J. Ptacek, Geochemistry of a permeable reactive barrier for metals and acid mine drainage, Environ. Sci. Technol. 33 (1999) 2793–2799.

[7] L.N. Daubert, R.A. Brennan, Passive remediation of acid mine drainage using crab shell chitin, Environ. Eng. Sci. 24 (2007) 1353–1358.

[8] K.M. Korte, C.E. Newcombe, R.A. Brennan, Evaluation of three different purities of crab-shell for the remediation of mine impacted water, in: R.I. Barnhisel (Ed.), Proceedings of the 25th National Meeting of the American Society of Mining and Reclamation, Richmond, VA, ASMR, Lexington, KY, June 14–19, 2008, pp. 510–524.

[9] M.A. Robinson-Lora, R.A. Brennan, Chitin complex for the remediation of mine impacted water: geochemistry of metal removal and comparison with other common substrates, Appl. Geochem. 25 (2010) 336–344.

[10] C. Venot, L. Figueroa, R.A. Brennan, T.R. Wildeman, D. Reisman, M. Sieczkowski, Comparing chitin and organic substrates on the National Tunnel Waters in Blackhawk, Colorado for manganese removal, in: R.I. Barnhisel (Ed.), Proceedings of the 25th National Meeting of the American Society of Mining and Reclamation, Richmond, VA, ASMR, Lexington, KY, June 14–19, 2008, pp. 1352–1366.

[11] A. Percot, C. Viton, A. Domard, Optimization of chitin extraction from shrimp shells, Biomacromolecules 4 (2003) 12–18.

[12] M.A. Robinson-Lora, Evaluation of chitinous materials as a multifunctional substrate for the remediation of mine impacted water, Ph.D. Dissertation. The Pennsylvania State University, State College, PA (2009).

[13] O. Gibert, J. de Pablo, J.L. Cortina, C. Ayora, Municipal compost-based mixture for acid mine drainage bioremediation: metal retention mechanisms, Appl. Geochem. 20 (2005) 1648–1657.

[14] C.M. Neculita, G.J. Zagury, B. Bussiere, Passive treatment of acid mine drainage in bioreactors using sulfate-reducing bacteria: critical review and research needs, J. Environ. Qual. 36 (2007) 1–16.

[15] J.S. Webb, S. McGuinnes, H.M. Lappin-Scott, Metal removal by sulfate-reducing bacteria from natural and constructed wetlands, J. Appl. Microbiol. 84 (1998) 240–248.

[16] M.A. Willow, R.R.H. Cohen, pH, dissolved oxygen, and adsorption effects on metal removal in anaerobic bioreactors, J. Environ. Qual. 32 (2003) 1212–1221.

[17] T. Zoumis, W. Calmano, U. Förer, Demobilization of heavy metals form mine waters, Acta Hydroch. Hydrob. 28 (2000) 212–218.

[18] M.M. Nassar, K.T. Ewida, E.E. Ebrahiem, Y.H. Magdy, Adsorption of iron and manganese ions using low-cost materials as adsorbents, Adsorpt. Sci. Technol. 22 (2004) 25–37.

[19] D. Mohan, S. Chander, Removal and recovery of metal ions from acid mine drainage using lignite—a low cost sorbent, J. Hazard. Mater. 137 (2006) 1545–1553.

[20] E. Chockalingam, S. Subramanian, Studies on removal of metal ions and sulfate reduction using rice husk and *Desulfotomaculum nifrificans* with reference to remediation of acid mine drainage, Chemosphere 62 (2005) 699–708.

[21] V. Utgikar, B. Chen, H.H. Tabak, D.F. Bishop, R. Govind, Treatment of acid mine drainage. I. Equilibrium biosorption of zinc and copper on non-viable activated sludge, Int. Biodeter. Biodegr. 46 (2000) 19–28.

[22] C.E. Newcombe, R.A. Brennan, Improved passive treatment of acid mine drainage in mushroom compost amended with crab-shell chitin, J. Environ. Eng. 136 (2010) 616–626.

[23] D.L. Parkhurst, C.A.J. Appelo, User's guide to PHREEQC (Version 2)—a computer program for speciation, batch-reaction, one-dimension transport and inverse geochemical calculations, U.S. Geological Survey Water-Resources Investigations Report 99-4259, 1999.

[24] W. Stumm, J.J. Morgan, Aquatic Chemistry: Chemical equilibria and Rates in Natural Waters, Wiley-Interscience, New York, 1996.

[25] J.S. Cox, D.S. Smith, L.A. Warren, F.G. Ferris, Characterizing heterogeneous bacterial surface functional groups using discrete affinity spectra for proton binding, Environ. Sci. Technol. 33 (1999) 4514–4521.

[26] F. Pagnanelli, F. Veglio, L. Toro, Modelling of the acid–base properties of natural and synthetic adsorbent materials used for heavy metal removal from aqueous solutions, Chemosphere 54 (2004) 905–915.

[27] G. Cardenas, G. Cabrera, E.S. Taboada, S.P. Patricia Miranda, Chitin characterization by SEM, FTIR, XRD, and ^{13}C cross polarization/mass angle spinning NMR, J. Appl. Polym. Sci. 93 (2004) 1876–1885.

[28] R. Dolphen, N. Sakkayawong, P. Thiravetyan, W. Nakbanpote, Adsorption of reactive red 141 from wastewater onto modified chitin, J. Hazard. Mater. 145 (2007) 250–255.

[29] B. Volesky, Z.R. Holan, Biosorption of heavy metals, Biotechnol. Prog. 11 (1995) 235–250.

[30] L.D. Franco, R.D.C. Maia, A.L.F. Porto, A.S. Messias, K. Fukushima, G.M. de Campos-Takaki, Heavy metal biosorption by chitin and chitosan isolated from *Cunninghamella elegans* (IFM 46109), Braz. J. Microbiol. 35 (2004) 243–247.

[31] G. Karthikeyan, N. Muthulakshmi Andal, K. Anbalagan, Adsorption studies of iron (III) on chitin, J. Chem. Sci. 117 (2005) 663–672.

[32] A. Moret, J. Rubio, Sulphate and molybdate ions uptake by chitin-based shrimp shells, Miner. Eng. 16 (2003) 715–722.

[33] H. Niu, B. Volesky, Characteristic of anionic metal species biosorption with waste crab shell, Hydrometallurgy 71 (2003) 209–215.

[34] D. Zhou, L. Zhang, S.L. Guo, Mechanisms of lead biosorption on cellulose/chitin beads, Water Res. 39 (2005) 3755–3762.

[35] D. Raabe, A. Al-Sawalmih, P. Romano, C. Sachs, H.G. Brokmeier, S.B. Yi, G. Servos, H.G. Hartwig, Structure and crystallographic texture of arthropod biocomposites, Mater. Sci. Forum 495–497 (2005) 1665–1674.

[36] M. Iijima, T. Hashimoto, Y. Matsuda, T. Nagai, Y. Yamano, T. Ichi, T. Osaki, S. Kawabata, Comprehensive sequence analysis of horseshoe crab cuticular proteins and their involvement in transglutaminase-dependent cross-linking, FEBS J. 272 (2005) 4774–4786.

[37] F. Shahidi, J. Synowiecki, Isolation and characterization of nutrients and value-added products from snow crab (*Chinoecetes opilio*) and shrimp (*Pandalus borealis*) processing discards, J. Agric. Food Chem. 39 (1991) 1527–1532.

[38] W.S.W. Ngah, S. Ab Ghani, A. Kamari, Adsorption behaviour of Fe(II) and Fe(III) ions in aqueous solution on chitosan and cross-linked chitosan beads, Bioresour. Technol. 96 (2005) 443–450.

[39] K. Vijayaraghavan, K. Palanivelu, M. Velan, Biosorption of copper(II) and cobalt(II) from aqueous solutions by crab shell particles, Bioresour. Technol. 97 (2006) 1411–1419.

[40] T.W. Webber, R.K. Chakravorti, Pore and solid diffusion models for fixed-bed adsorbers, AIChE J. 20 (1974) 228–238.

[41] E. Pretsch, P. Bühlmann, M. Badertscher, Structure Determination of Organic Compounds: Tables of Spectral Data, 4th ed., Springer, Berlin, Heidelberg, 2009.

[42] B. Focher, A. Naggi, G. Torri, A. Cosani, M. Terbojevich, Structural differences between chitin polymorphs and their precipitates from solutions—evidence from CP-MAS ^{13}C NMR, FT-IR and FT-Raman spectroscopy, Carbohyd. Polym. 17 (1992) 97–102.

[43] D.M. Byler, H. Susi, Examination of the secondary structure of proteins by deconvolved FTIR spectra, Biopolymers 25 (1986) 469–487.

[44] J.C.P. Vaghetti, E.C. Lima, B. Royer, B.M. da Cunha, N.F. Cardoso, J.L. Brasil, S.L.P. Dias, Pecan nutshell as biosorbent to remove Cu(II), Mn(II) and Pb(II) from aqueous solutions, J. Hazard. Mater. 162 (2009) 270–280.

[45] K. Vijayaraghavan, T.T. Teo, R. Balasubramanian, U.M. Joshi, Application of *Sargassum* biomass to remove heavy metal ions from synthetic multi-metal solutions and urban storm water runoff, J. Hazard. Mater. 164 (2009) 1019–1023.

[46] B. Benguella, H. Benaissa, Cadmium removal from aqueous solutions by chitin: Kinetic and equilibrium studies, Water Res. 36 (2002) 2463–2474.

[47] I.B. Rae, S.W. Gibb, Removal of metals from aqueous solutions using natural chitinous materials, Water Sci. Technol. 47 (2003) 189–196.

[48] M.A. Robinson-Lora, R.A. Brennan, The use of crab-shell chitin for biological denitrification: Batch and column tests, Bioresour. Technol. 100 (2009) 534–541.

[49] H.K. An, B.Y. Park, D.S. Kim, Crab shell for the removal of heavy metals from aqueous solution, Water Res. 35 (2001) 3551–3556.

[50] Moo-Yeal Lee, Kyung-Jin Hong, Toshio Kajiuchi, Ji-Won Yang, Determination of the efficiency and removal mechanism of cobalt by crab shell particles, J. Chem. Technol. Biotechnol. 79 (2004) 1388–1394.

[51] M. Sheela, Doshi, Bioremediation of Acid Mine Drainage Using Sulfate-reducing Bacteria, U.S. Environmental Protection Agency, 2006.